

Quaternary structures of tumor suppressor p53 and a specific p53–DNA complex

Henning Tidow*, Roberto Melero†, Efstratios Mylonas‡, Stefan M. V. Freund*, J. Guenter Grossmann§, José María Carazo†, Dmitri I. Svergun¶||, Mikel Valle†||**, and Alan R. Fersht*||

*Medical Research Council Centre for Protein Engineering, Hills Road, Cambridge CB2 0QH, United Kingdom; †Centro Nacional de Biotecnología, Darwin 3, Cantoblanco 28049 Madrid, Spain; **CIC-bioGUNE, Parque Tecnológico de Bizkaia, 48160 Derio, Spain; ‡European Molecular Biology Laboratory, Hamburg Outstation, Notkestrasse 85, 22603 Hamburg, Germany; †Institute of Crystallography, Russian Academy of Sciences, Leninsky pr. 59, 117333 Moscow, Russia; and §Molecular Biophysics Group, Council for the Central Laboratory of the Research Councils (CCLRC) Daresbury Laboratory, Warrington, Cheshire WA4 4AD, United Kingdom

Contributed by Alan R. Fersht, May 30, 2007 (sent for review May 8, 2007)

The homotetrameric tumor suppressor p53 consists of folded core and tetramerization domains, linked and flanked by intrinsically disordered segments that impede structure analysis by x-ray crystallography and NMR. Here, we solved the quaternary structure of human p53 in solution by a combination of small-angle x-ray scattering, which defined its shape, and NMR, which identified the core domain interfaces and showed that the folded domains had the same structure in the intact protein as in fragments. We combined the solution data with electron microscopy on immobilized samples that provided medium resolution 3D maps. *Ab initio* and rigid body modeling of scattering data revealed an elongated cross-shaped structure with a pair of loosely coupled core domain dimers at the ends, which are accessible for binding to DNA and partner proteins. The core domains in that open conformation closed around a specific DNA response element to form a compact complex whose structure was independently determined by electron microscopy. The structure of the DNA complex is consistent with that of the complex of four separate core domains and response element fragments solved by x-ray crystallography and contacts identified by NMR. Electron microscopy on the conformationally mobile, unbound p53 selected a minor compact conformation, which resembled the closed conformation, from the ensemble of predominantly open conformations. A multipronged structural approach could be generally useful for the structural characterization of the rapidly growing number of multidomain proteins with intrinsically disordered regions.

DNA binding | intrinsically unfolded | modular | natively disordered | protein

The tumor suppressor p53 is a tetrameric, multidomain transcription factor that plays a central role in the cell cycle and maintaining genomic integrity (1, 2). It binds to specific DNA response elements, is integrated in various signaling networks by a multitude of protein–protein interactions, and is controlled by extensive posttranslational modifications (1, 3, 4). p53 protein is a homotetramer of 4×393 residues. Each chain consists of two folded domains [the core, or DNA-binding, domain (94–294) and the tetramerization domain (323–360)] that are linked by an intrinsically disordered sequence. The transactivation domain (1–67) (5), proline-rich region (67–94), nuclear localization signal (NLS)-containing region (303–323) (6), and C-terminal negative regulatory domain (360–393) are also intrinsically disordered (7–9) (see refs. 10 and 11 for reviews). The DNA-binding core domain (residues 94–294) binds to sequence-specific response elements associated with p53 target gene promoters (12–14). The structures of the core domain complexes with DNA have been solved by crystallography (15–17), and in solution in the absence of DNA by NMR (18). The structure of the tetramerization domain has been solved by both NMR and x-ray crystallography (19–21).

Structural studies on full-length p53 have been impeded both by its intrinsic instability and the presence of disordered regions

(8, 18, 22, 23). There is an increasing number of proteins being discovered to have globular domains linked by intrinsically disordered regions (24), and so the determination of such structures will be a recurring problem. Recently, the first structure of full-length murine p53, obtained by cryoelectron microscopy, was reported (25). It gave a radically new concept of the molecular organization of p53. We have solved the instability problem of human p53 by designing a biologically active mutant with a superstable core domain (26, 27) that is suitable for NMR studies. NMR studies have given a picture of the p53 tetramer as a dimer of loosely tethered core dimers of appropriate symmetry to be poised to bind target DNA with well resolved transverse relaxation optimized spectroscopy (TROSY) NMR spectra (23). But, on addition of DNA, the protein rigidifies with poorly resolved spectra (23).

Here, we used small-angle x-ray scattering (SAXS), electron microscopy (EM), and NMR spectroscopy in a multitechnique approach to determine the structures of tetrameric full-length human p53 and various truncation mutants, both unligated and as a complex with a DNA response element.

Results and Discussion

Quaternary Structure of p53 from SAXS. SAXS experiments were performed on solutions of three p53 constructs: p53 core plus tetramerization domain (94–360) (CTetD), p53 core plus tetramerization plus C-terminal domain (94–393) (CTetCD), and full-length p53 (1–393) (flp53). All had four stabilizing mutations in the core domain (M133L/V203A/N239Y/N268D) (27) that do not perturb the structure (26). The processed experimental patterns (scattering intensity I versus momentum transfer $s = 4\pi\sin\theta/\lambda$, where 2θ is the scattering angle and $\lambda = 1.5 \text{ \AA}$ is the wavelength) are displayed in Fig. 1*a*, and the overall parameters are summarized in Table 1. The solutions are monodisperse [supporting information (SI) Fig. 6], and the molecular weights (M_r) of the solutes determined from the extrapolated zero angle intensity $I(0)$ consistently point to a tetrameric assembly for each construct. The radius of gyration (R_g) increases from CTetD (52.2 Å) to CTetCD (54.0 Å) to flp53 (68.2 Å) (Table 1). The

Author contributions: H.T. and R.M. contributed equally to this work; H.T., R.M., E.M., S.M.V.F., J.M.C., M.V., and A.R.F. designed research; H.T., R.M., E.M., S.M.V.F., J.G.G., and M.V. performed research; H.T., R.M., E.M., S.M.V.F., J.M.C., D.I.S., M.V., and A.R.F. analyzed data; and H.T., D.I.S., M.V., and A.R.F. wrote the paper.

The authors declare no conflict of interest.

Abbreviations: CTetD, p53 core and tetramerization domains; CTetCD, p53 core, tetramerization and C-terminal domain; flp53, full-length p53; SAXS, small-angle X-ray scattering; TROSY, transverse relaxation optimized spectroscopy.

See Commentary on page 12231.

||To whom correspondence may be addressed. E-mail: arf25@cam.ac.uk, mvalle@cicbiogune.es, or svergun@embl-hamburg.de.

This article contains supporting information online at www.pnas.org/cgi/content/full/0705069104/DC1.

© 2007 by The National Academy of Sciences of the USA

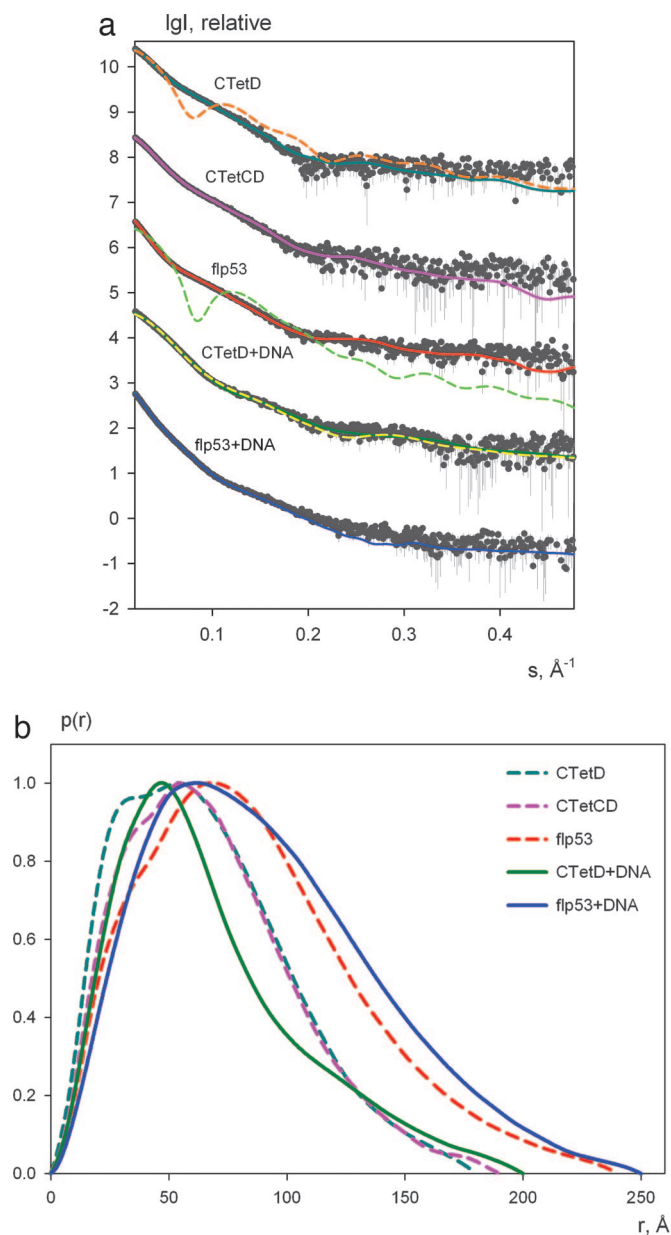


Fig. 1. SAXS analysis of p53 constructs. (a) Experimental intensities (dots with error bars) and fits computed from the structural models by rigid body modeling: CTetD (cyan), CTetCD (magenta), flp53 (red), CTetD+DNA (dark green). For the flp53–DNA complex the fit from the *ab initio* model (SI Fig. 9) is displayed in blue. The scattering profiles are displaced along the ordinate for better visualization. The fit to the CTetD data from the model proposed by Okorokov *et al.* (25) and the fit to flp53 data from the EM-map by Okorokov *et al.* (25) are shown in dashed orange and dashed light green, respectively. The fit to our EM-based model is shown in dashed yellow. (b) The distance distribution plots computed from the experimental data and normalized to the maximum value of unity.

distance distribution functions of all of the constructs display peaks or shoulders at shorter distances (20–50 Å), indicating the presence of separated subdomains (Fig. 1b). CTetCD reveals only small expansion of the structure compared with CTetD, whereas flp53 demonstrates a significant increase in the overall dimensions (Table 1). This increase indicates that the N-terminal domain is not folded back onto the core protein but instead is largely extended and potentially flexible (although, as evidenced by the so-called Kratky plot in SI Fig. 7, not completely un-

Table 1. Overall parameters of p53 constructs determined by SAXS

Construct	R_g , Å	D_{max} , Å	Mass, kDa*
p53 CTetD	52.2 ± 0.4	180 ± 10	105 ± 10 (120)
p53 CTetCD	54.0 ± 0.3	190 ± 15	118 ± 12 (134)
Full-length p53	68.2 ± 0.3	240 ± 30	199 ± 20 (175)
p53 CTetD + DNA	52.8 ± 0.5	200 ± 20	140 ± 15 (135)
flp53 + DNA	72.3 ± 0.8	250 ± 30	290 ± 40 (190)

R_g , radius of gyration; D_{max} , maximum size of particle.

*Mass values were evaluated by normalization against the BSA solution accounting for the contrast reduction due to 5% glycerol and (for the DNA-containing constructs) also for the higher DNA contrast compared with that of the protein. In parentheses, the expected masses of tetrameric constructs are given.

folded). This finding agrees with NMR results showing that the N-terminal region within the full-length protein is flexible (S.M.V.F. and A.R.F., unpublished results).

Low-resolution DAMMIN (28) revealed elongated cross-shaped structures (a typical model is displayed in SI Fig. 8). There are only small changes in chemical shifts of the core and tetramerization domains in flp53 compared with separate domains in solution (23). Accordingly, the known high-resolution structures of p53 core (PDB ID code: 1TUP, 2AC0) and tetramerization domains (PDB ID code: 1C26) were used to build models of p53 constructs by using the programs SASREF and BUNCH (29). These programs perform rigid-body refinement against single or multiple data sets but also allow one to model the missing linkers as dummy residue chains. The configuration of the tetramerization domain was fixed as in the crystal structure, and the linkers and core domains were added to fit the experimental data assuming the P222 symmetry of the constructs. Independently determined models of all constructs consistently display extended cross-like structures, their overall shape being compatible with the *ab initio* reconstructions (SI Fig. 8). Importantly, the tetramerization domain in the middle of these models is surrounded by two pairs of associated core domains, which is consistent with previous NMR results on the mobility of core domains (23).

To constrain the modeling further, we fitted the three scattering patterns from CTetD, CTetCD, and flp53 simultaneously and added information about the interacting surface of the core dimers. The residues likely to be involved in domain interfaces are found from comparing chemical shifts in the tetrameric constructs with those in isolated core domains (23). The interface found previously (23) has now been reassigned to that of the interaction of core domain in flp53 with its N-terminal extension (S.M.V.F., C. Baloglu, and A.R.F., unpublished results). The interface between the core domains in the crystal structure of the complex of p53 monomers with DNA has self-complementarity of residues 177, 178, 180, 181, 243, and 244 (17). These residues are also implicated in the NMR spectra of dimeric constructs of two core domains with half-site DNA (30, 31). Signals for residues 181, 243, and 244 are in clear isolated positions in the 800 and 900 MHz ^1H - ^{15}N TROSY spectrum of core domain (Fig. 2). Although there are insignificant changes in chemical shifts of nearly all of the remaining 147 assigned residues of the core domain in CTetD relative to core, the signals from 181, 243, and 244 are missing. We attribute the absence of those signals to line broadening from chemical exchange as each pair of core domains associates and dissociates, lowering the signals below the threshold for detection. Further, the normalized changes in ^1H - ^{15}N chemical shifts for 178 and 179 are among the two greatest in the spectrum at 0.034 and 0.059 ppm, respectively. These data are compatible with a transient inter-

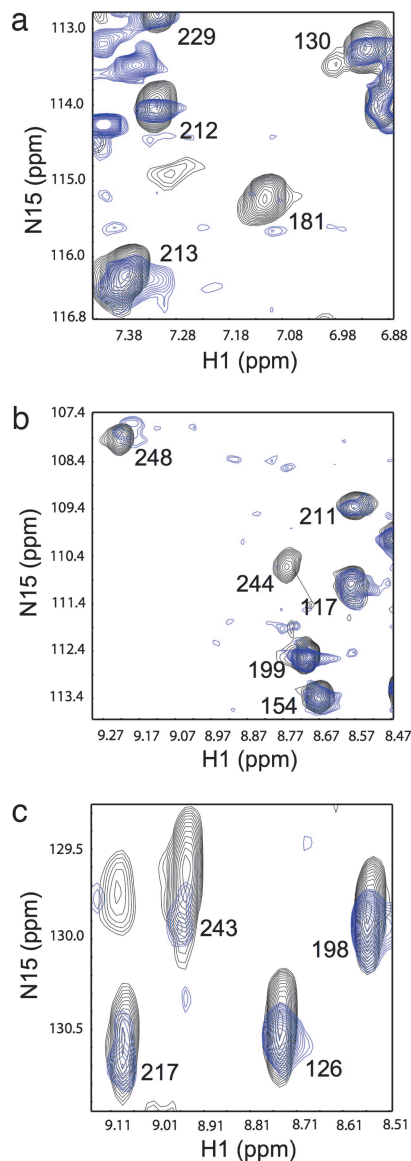


Fig. 2. Overlay of TROSY spectra acquired for p53 core domain (black) and p53 CTetD (blue) of 100- μ M samples. Chemical shift deviations for the p53 CTetD spectra were estimated from the overlay and partly confirmed with TROSY-based triple resonance spectra (data not shown). Most of the core resonances showed insignificant chemical shift deviations between the two spectra. The expansions *a*, *b*, and *c* show signals that are strong and well isolated in the spectrum of isolated core domains but are not seen in the spectrum of CTetD most likely because of substantial line broadening associated with residues in a protein–protein interface. In *a* 181 and in *b* 244 are lost, and in *c* 243 is severely diminished. Spectra were plotted close to the noise level; additional signals in *a* are from the linker region between core and tetramerization domain.

action between core domains involving the same interface observed in the crystal structure of the core domain–DNA complex (17).

We included the interface detected by NMR constraints, using the crystal structure coordinates (17). A typical constrained model displayed in Fig. 3 fits simultaneously the scattering patterns from CTetD, CTetCD, and flp53 with discrepancy $\chi = 0.82, 0.83,$ and $1.24,$ respectively (Fig. 3). The overall shape of this model is compatible with those of the unconstrained model and with the *ab initio* model (SI Fig. 8), but the constrained model displays a somewhat different orientation of the core domains.

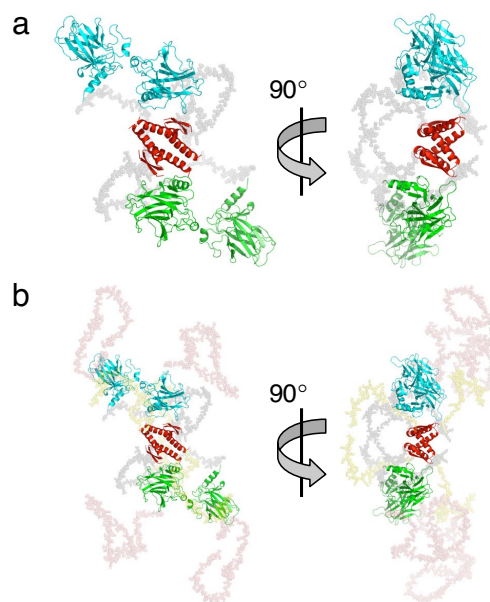


Fig. 3. SAXS models of free p53 in solution from rigid body analysis and addition of missing fragments. (a) CTetD portion of flp53 shown in *b*. Core domains and tetramerization domain are displayed in cartoon representation, connecting linkers (gray), N termini (salmon), and C termini (yellow) in semitransparent spacefill mode. Both models are presented in two orthogonal views. The model of flp53 and its CTetD and CTetCD portions fit simultaneously the experimental SAXS data from appropriate constructs in Fig. 1*a*.

The C termini are located in the central part surrounding the tetramerization domain, whereas the N-terminal domains are rather extended and point toward the periphery of the molecule.

It cannot be excluded that p53 has a considerable degree of conformational flexibility in solution and that the SAXS-generated models represent an average over such an ensemble. The conformation of potentially flexible linkers and termini, in particular in Fig. 3*b*, should be taken only as an indication of the volume occupied by these chains. On the other hand, the configuration of the tetramerization and core domains in CTetD appears rather rigid and reproducibly reconstructed in the independent modeling of different constructs. Summarizing, the model in Fig. 3 is compatible with a large body of SAXS and NMR evidence. In contrast, the calculated scattering from the recently published EM structure of p53 (25) does not agree with experimental SAXS data, yielding a poor fit with $\chi = 9.2$ (Fig. 1*a*).

Structure of p53–DNA Complex from SAXS. Tetrameric flp53 and CTetD bind 24-residue *gadd45* or *p21* response element DNA with K_d in the low nanomolar range (32, 33). The scattering profiles from the DNA complexes are displayed in Fig. 1*a* and the overall parameters are summarized in Table 1. The CTetD–DNA complex is clearly compatible with tetrameric CTetD and a single DNA molecule, whereas the M_r of the flp53–DNA complex somewhat exceeds the expected value, which may point to some aggregation or high flexibility. The distance distributions of DNA complexes display no “fine-structure” at small distances observed for free p53 constructs, suggesting that the internal structure of the complexes is more compact than that of free protein (Fig. 1*b*). This compaction is further confirmed by comparison of the Kratky plots of the free and DNA-bound p53 constructs (SI Fig. 7).

We generated the structural model for the CTetD–DNA complex by rigid body modeling using the core domains, tetramerization domain, and DNA. This procedure yielded two

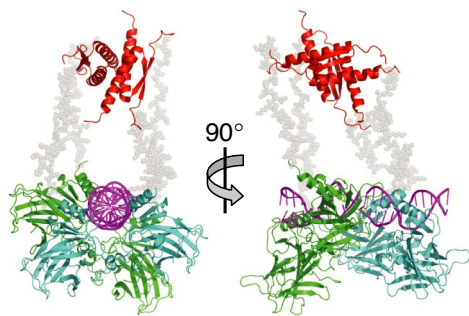


Fig. 4. Rigid body model of a p53–DNA complex from SAXS data. Core domains, tetramerization domain and DNA are shown in cartoon representation, connecting linkers in semitransparent spacefill mode. The model is displayed in two orthogonal views.

types of alternative models both showing four core domains binding to DNA and a tetramerization domain in its tetrameric form. These two structures fit the experimental data equally well and differ only by the positioning of the tetramerization domain with respect to the core domains–DNA complex (data not shown). Because one SAXS model was very similar to our EM model (see *Structure of p53–DNA Complex from EM*), we used this latter model as a starting point to add missing linkers and termini that could not be visualized in the EM map. The final model of the CTetD–DNA complex fitting the experimental data with $\chi = 1.48$ (Fig. 1*a*) reveals two superdomains: four core domains bound to DNA as described by Kitayner *et al.* (17), and the tetramerization domain (Fig. 4). These superdomains are separated by 40–120 Å and connected by linkers. The full-length p53–DNA complex appears much more extended than the CTetD–DNA complex (Table 1), suggesting that the N terminus is extremely extended. This extended structure agrees with the TROSY-NMR spectra on these complexes, which show that the N-terminal resonances remain unchanged (ref. 23). Attempts to add the missing termini yielded poor fits to the scattering pattern from the flp53–DNA complex, suggesting that the N termini may be even more flexible than those in the free-full length p53 (as indicated above, aggregation could also not be excluded). A tentative model of the flp53–DNA complex constructed *ab initio* by DAMMIN accommodates the rigid-body model of the CTetD–DNA complex and leaves ample space for the missing termini (SI Fig. 9).

Structure of p53 from EM. The EM images for negative-stained flp53 were heterogeneous in shape and size, and so the global set was unsuitable for 3D averaging techniques. A fraction, <20%, of the total particles adsorbed to the carbon support layer, however, was compact, with uniform structures of a size that was compatible with 2D projections of flp53 tetramers. We calculated the 3D map for this group following a reference-free scheme and imposing an overall C2 symmetry (see *SI Materials and Methods* and SI Fig. 10). At the defined density threshold, the map reveals a structure with two main masses linked by two faint connecting regions (SI Fig. 10*a* and *b*). Despite the limitations of the negative staining approach and the moderate resolution of the 3D map (estimated in the range of 25–30 Å), the boundaries allowed us to fit available atomic coordinates for p53 core (15, 17) and tetramerization (19, 20) domains. The 3D map (SI Fig. 10*d–f*) resembles and accommodates both structures with no need of major rearrangements, and the C termini of the core domains point toward the tetramerization domains for their connection. This structure is not the major one in solution that was found from the SAXS studies, and the computed scattering pattern does not match the experimental profile from CTetD ($\chi = 4.37$). It may well be that this is a genuine low

occupancy conformation that has to open to allow access of DNA to the binding site.

Structure of p53–DNA Complex from EM. EM images of stained flp53 in a complex with a 60-bp dsDNA probe containing a sequence-specific binding site DNA had a more uniform size distribution than the unligated protein. The volume, rendered from the calculated 3D map (Fig. 5*a–c*), does not show the dsDNA. This invisibility is a typical drawback of negative stained protein–nucleic acid samples, where nucleic acids (thin and charged strings) are rarely visible and sometimes positively stained. The EM map, however, contains structural features that confirm the presence of the DNA probe, and we independently confirmed the presence of the flp53–DNA complex by EMSA (data not shown).

As with the EM structure of free flp53, there were two regions of density, at the top and bottom, ≈ 40 Å apart, connected by two linkers (Fig. 5*a* and *b*). Importantly, the connecting densities in the map for p53–DNA complex were more obvious than for the free flp53 (see SI Fig. 10*a* and *b* and Fig. 5*a* and *b*) and were retained at high cut-off density thresholds. Those densities clearly delineate a see-through channel with the shape of a circle in one of the side views (Fig. 5*a*). The crystal structure of four core domains bound to dsDNA (17) fits very well around the channel of missing density of DNA (Fig. 5*d*). The EM map is understood as of a stained flp53 tetramer wrapped around unstained dsDNA.

The fitted atomic structures for the core (17) and tetramerization domains (19) are consistent with the EM envelope for the p53–DNA complex (Fig. 5*d–f*). Importantly, the SAXS pattern computed from the complete EM-based model, including the core and tetramerization domains and the DNA, is fully consistent with the experimentally measured scattering data from CTetD+DNA construct (Fig. 1*a*, dashed yellow curve; the fit neatly is graphically indistinguishable from the dark green curve). A local disagreement is seen for two of the core domains that protrude outside the 3D map exposing their C-terminal region (apparent for the right cyan monomer in Fig. 5*d*). We have used the atomic coordinates as rigid bodies, and no alternative arrangement is presented. Some differences between our p53–DNA complex and the crystallographic structure of the core domain tetramer bound to DNA (17) could explain this discrepancy. The x-ray structure was determined for the isolated core domain tetramer and in complex with two DNA molecules, whereas our p53–DNA sample covers the entire protein bound to a unique DNA probe. However, we cannot rule out either a partial distortion of the p53–DNA structure because of the aggressive nature of the negative staining technique.

Kitayner *et al.* (17) modeled the structure of flp53 bound to DNA based on their crystal structure of four core domains bound to two segments of DNA and the positions of where the linker sections to the tetramerization domain would exit the truncated structure. The relative positions of core and tetramerization domains are in excellent agreement with the structures determined here by both SAXS and EM.

General Implications for Structure Determination. p53 is typical of the class of proteins containing a mixture of ordered and disordered domains. The strategy used here of fitting the high resolution structures of individual domains, solved by x-ray crystallography or NMR, into low resolution SAXS and EM data, guided by TROSY NMR constraints on interfaces, may well be a useful general approach to solving their structures. SAXS, like conventional NMR spectroscopy, has the advantage of analyzing structures in solution, obviating any artifacts associated with freezing of samples or immobilizing them on a grid, as used in EM. However, it does not generate unique models. SAXS optimizes the spatial arrangement of subunits by direct

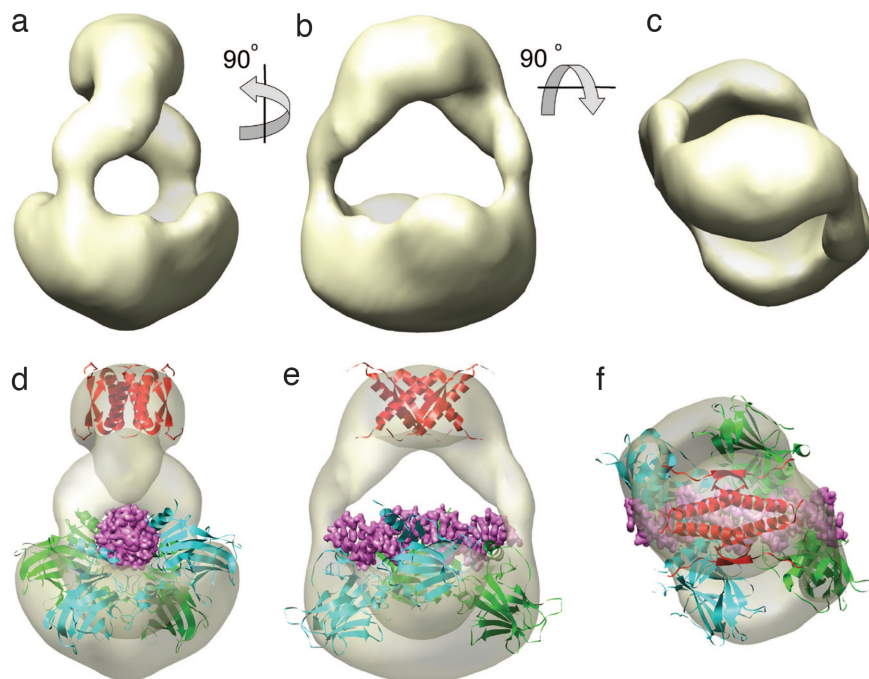


Fig. 5. 3D-EM map for flp53-DNA complex. The 3D map for the p53-DNA complex is rendered with a volume that covers 100% of the expected volume for a p53 tetramer in solid (a–c) and semitransparent (d–f) views. The fitted coordinates place the representation for the dsDNA in the see-through channel of one of the side views (see a and d).

fitting of experimental scattering data on docking high-resolution structures into shapes of macromolecular complexes, but there may be more than one solution (29). EM of negative stained samples uses an envelope obtained after 3D image reconstruction for docking of high-resolution models of subunits, and the overall shape should not be ambiguous if the high-resolution structures of domains are assigned correctly in the envelope. However, immobilization on the carbon support and differential staining may lead to selection of a particular conformation. SAXS data are particularly useful for discriminating between independently determined models by comparing calculated and observed scattering profiles because SAXS can eliminate incorrect models (34), and differences between SAXS solution models and EM-generated models have been reported (35). The differences between the structures of unligated p53 determined in solution and by EM show that a multimethod approach is necessary.

It is striking, here, that both EM and SAXS generate a very similar model for a p53-DNA complex, which is a relatively rigid structure. For the free p53, however, the solution studies using SAXS and NMR indicate a structure of loosely tethered pairs of core domains, with the possibilities of facile conformational rearrangement. Our EM studies, in contrast, show a structure that is preformed for binding the DNA response element. However, the calculated scattering profile is inconsistent with that found from the overall population in solution. It is likely that the experimental conditions for EM have selected a minor closed conformation that has to open for DNA to have access to the binding site. The model proposed for murine p53 (25) may also be a minor closed conformation. Key features of the murine model are not consistent with our data: for example, the murine model has the tetramerization domain dissociated and the N and C termini in contact. We find from SAXS that unligated p53 and its truncation variants all have the same quaternary arrangements of core and tetramerization domains, showing that the structure does not depend on the interaction of the N and C termini. Further, the dissociation constants of flp53 and CTetD

lacking the C and N termini are quite similar (23). For the conformationally flexible free p53, the structures from SAXS, with supplementary information from NMR, must have precedence over the structures purely from EM.

Biological Relevance of the Quaternary Structure. The presence of an extended N-terminal domain in our model is consonant with its biological function. The N-terminal domain of p53 is subject to extensive posttranslational modifications that potentially regulate transactivational activity (36, 37). It also binds to a variety of proteins that further modulate p53 activity, like MDM2 (38), p300 (39), several transcription activators of the TFIID complex (40–42), and RPA (43). Upon binding to other proteins, small regions within the intrinsically unfolded p53 N terminus form helical structures (38, 43), a phenomenon also observed for other transcription factors (44–46). Further, our model of loosely coupled core domains assembled in an elongated cross-shaped structure allows binding of regulatory protein like Bcl-xL (47), Bcl2 (48), or 53BP2 (49, 50) to p53 core domain.

The open arrangement in flp53 of two separate pairs of core domains (Fig. 3) allows access of DNA to the binding site: first, one pair of core domains binds to two of the four binding site on a response element; then, the flexible linkers between the core and tetramerization domains allow the second pair of core domains to bind to the remaining two sites, thus burying the DNA within the protein.

Methods

Human p53 CTetD, CTetCD, and full-length p53 were expressed in *Escherichia coli* and purified as described (23). SAXS data were collected at the X33 beamline at European Molecular Biology Laboratory/Deutsches Elektronen Synchrotron (EMBL/DESY), Hamburg and at station 2.1 of the Daresbury Synchrotron Radiation Source (SRS) following standard procedures. Electron microscopy using negative staining involved manual selection of particles and reference-free classification (see SI Fig. 11). TROSY NMR spectra were acquired on 800

MHz and 900 MHz spectrometers by using perdeuterated, isotopically ^2H , ^{15}N -labeled samples. Details of sample preparation, SAXS measurements and modeling, electron microscopy, image processing and domain fitting, and NMR spectroscopy are given in *SI Materials and Methods*.

We thank Dr. A. Joerger for helpful discussions, C. Blair (MRC Centre for Protein Engineering, Cambridge, U.K.) for TEV protease and protein preparation, Dr. E. Orlova for communication of coordinates of murine p53 and kind comments, Dr. J. Milner for kind comments, and Dr. R. Nuñez for help using EMAN. M.V. is supported by Spanish

Ministry of Education and Science Grant BFU2006-09648, by Etorrek Research Programs 2005/2006 (The Department of Industry, Tourism and Trade of the Government of the Autonomous Community of the Basque Country), and by the Innovation Technology Department of the Bizkaia County. H.T. is supported by a fellowship from the Boehringer Ingelheim Fonds. We acknowledge support from European Community–Research Infrastructure Action under the FP6 (RII3/CT/2004/5060008) for access to EMBL/DESY, Hamburg, and access to the European Large Scale Facility for NMR Spectroscopy in Utrecht, The Netherlands. D.I.S. and J.G.G. acknowledge support from the European Union FP6 Design Study Small-Angle X-Ray Scattering Initiative for Europe (SAXIER), RIDS 011934.

- Hainaut P, Wiman KG, eds (2005) *25 Years of p53 Research* (Springer, New York).
- Vogelstein B, Lane D, Levine AJ (2000) *Nature* 408:307–310.
- Hupp TR, Lane DP (1994) *Cold Spring Harbor Symp Quant Biol* 59:195–206.
- Hupp TR, Sparks A, Lane DP (1995) *Cell* 83:237–245.
- Dawson R, Muller L, Dehner A, Klein C, Kessler H, Buchner J (2003) *J Mol Biol* 332:1131–1141.
- Shaalsky G, Goldfinger N, Ben-Ze'ev A, Rotter V (1990) *Mol Cell Biol* 10:6565–6577.
- Ayed A, Mulder FA, Yi GS, Lu Y, Kay LE, Arrowsmith CH (2001) *Nat Struct Biol* 8:756–760.
- Bell S, Klein C, Muller L, Hansen S, Buchner J (2002) *J Mol Biol* 322:917–927.
- Lee H, Mok KH, Muhandiram R, Park KH, Suk JE, Kim DH, Chang J, Sung YC, Choi KY, Han KH (2000) *J Biol Chem* 275:29426–29432.
- Joerger AC, Fersht AR (2007) *Oncogene* 26:2226–2242.
- Roemer L, Klein C, Dehner A, Kessler H, Buchner J (2006) *Angew Chem Int Ed Engl* 45:6440–6460.
- el-Deiry WS, Kern SE, Pietenpol JA, Kinzler KW, Vogelstein B (1992) *Nat Genet* 1:45–49.
- Kern SE, Kinzler KW, Bruskin A, Jarosz D, Friedman P, Prives C, Vogelstein B (1991) *Science* 252:1708–1711.
- Wei CL, Wu Q, Vega VB, Chiu KP, Ng P, Zhang T, Shahab A, Yong HC, Fu Y, Weng Z, et al. (2006) *Cell* 124:207–219.
- Cho Y, Gorina S, Jeffrey PD, Pavletich NP (1994) *Science* 265:346–355.
- Ho WC, Fitzgerald MX, Marmorstein R (2006) *J Biol Chem* 281:20494–20502.
- Kitayner M, Rozenberg H, Kessler N, Rabinovich D, Shaulov L, Haran TE, Shakked Z (2006) *Mol Cell* 22:741–753.
- Canadillas JM, Tidow H, Freund SM, Rutherford TJ, Ang HC, Fersht AR (2006) *Proc Natl Acad Sci USA* 103:2109–2114.
- Clore GM, Omichinski JG, Sakaguchi K, Zambrano N, Sakamoto H, Appella E, Gronenborn AM (1995) *Science* 267:1515–1516.
- Jeffrey PD, Gorina S, Pavletich NP (1995) *Science* 267:1498–1502.
- Lee W, Harvey TS, Yin Y, Yau P, Litchfield D, Arrowsmith CH (1994) *Nat Struct Biol* 1:877–890.
- Bullock AN, Henckel J, DeDecker BS, Johnson CM, Nikolova PV, Proctor MR, Lane DP, Fersht AR (1997) *Proc Natl Acad Sci USA* 94:14338–14342.
- Vepritsnev DB, Freund SM, Andreeva A, Rutledge SE, Tidow H, Canadillas JM, Blair CM, Fersht AR (2006) *Proc Natl Acad Sci USA* 103:2115–2119.
- Dyson HJ, Wright PE (2002) *Curr Opin Struct Biol* 12:54–60.
- Okorokov AL, Sherman MB, Plisson C, Grinkevich V, Sigmundsson K, Selivanova G, Milner J, Orlova EV (2006) *EMBO J* 25:5191–5200.
- Joerger AC, Allen MD, Fersht AR (2004) *J Biol Chem* 279:1291–1296.
- Nikolova PV, Henckel J, Lane DP, Fersht AR (1998) *Proc Natl Acad Sci USA* 95:14675–14680.
- Svergun DI (1999) *Biophys J* 76:2879–2886.
- Petoukhov MV, Svergun DI (2005) *Biophys J* 89:1237–1250.
- Klein C, Planker E, Diercks T, Kessler H, Kunkele KP, Lang K, Hansen S, Schwaiger M (2001) *J Biol Chem* 276:49020–49027.
- Rippin TM, Freund SM, Vepritsnev DB, Fersht AR (2002) *J Mol Biol* 319:351–358.
- Ang HC, Joerger AC, Mayer S, Fersht AR (2006) *J Biol Chem* 281:21934–21941.
- Weinberg RL, Vepritsnev DB, Fersht AR (2004) *J Mol Biol* 341:1145–1159.
- Vestergaard B, Sanyal S, Roessle M, Mora L, Buckingham RH, Kastrup JS, Gajhede M, Svergun DI, Ehrenberg M (2005) *Mol Cell* 20:929–938.
- Pioletti M, Findeisen F, Hura GL, Minor DL, Jr (2006) *Nat Struct Mol Biol* 13:987–995.
- Banin S, Moyall L, Shieh S, Taya Y, Anderson CW, Chessa L, Smorodinsky NI, Prives C, Reiss Y, Shiloh Y, Ziv Y (1998) *Science* 281:1674–1677.
- Shieh SY, Ikeda M, Taya Y, Prives C (1997) *Cell* 91:325–334.
- Kussie PH, Gorina S, Marechal V, Elenbaas B, Moreau J, Levine AJ, Pavletich NP (1996) *Science* 274:948–953.
- Grossman SR (2001) *Eur J Biochem* 268:2773–2778.
- Lu H, Levine AJ (1995) *Proc Natl Acad Sci USA* 92:5154–5158.
- Naar AM, Lemon BD, Tjian R (2001) *Annu Rev Biochem* 70:475–501.
- Thut CJ, Chen JL, Klemm R, Tjian R (1995) *Science* 267:100–104.
- Bochkareva E, Kaustov L, Ayed A, Yi GS, Lu Y, Pineda-Lucena A, Liao JC, Okorokov AL, Milner J, Arrowsmith CH, Bochkarev A (2005) *Proc Natl Acad Sci USA* 102:15412–15417.
- Bowers PM, Schaufler LE, Klevit RE (1999) *Nat Struct Biol* 6:478–485.
- Graham TA, Weaver C, Mao F, Kimelman D, Xu W (2000) *Cell* 103:885–896.
- Spolar RS, Record MT, Jr (1994) *Science* 263:777–784.
- Chipuk JE, Bouchier-Hayes L, Kuwana T, Newmeyer DD, Green DR (2005) *Science* 309:1732–1735.
- Tomita Y, Marchenko N, Erster S, Nemajero A, Dehner A, Klein C, Pan H, Kessler H, Pancoska P, Moll UM (2006) *J Biol Chem* 281:8600–8606.
- Gorina S, Pavletich NP (1996) *Science* 274:1001–1005.
- Tidow H, Vepritsnev DB, Freund SM, Fersht AR (2006) *J Biol Chem* 281:32526–32533.